International Journal of Multidisciplinary Research and Growth Evaluation.

Hybrid Jellyfish Search and Gradient Boosting Optimizer for Exergo-Economic Optimization of Nanofluid-Based PV/T Systems Integrated with Thermoelectric Generators

Ali Najah Kadhim
Al-Furat Al-Awsat Technical University, Kufa, Najaf, Iraq

* Corresponding Author: **Ali Najah Kadhim**

Article Info

ISSN (Online): 2582-7138
Volume: 07
Issue: 04
Received: 13-05-2026
Accepted: 15-06-2026
Published: 17-07-2026
Page No: 867-882

Abstract
Photovoltaic/thermal (PV/T) systems are used to produce electricity and useful heat from solar radiation. They are influenced by coupled thermal, hydraulic, exergetic, and economic interactions. The synergistic effect of the nanofluid concentration, pumping power, collector area, and thermoelectric-generator (TEG) operating modes is not fully captured by the independent optimization studies based on a single parameter. For this purpose, a hybrid Jellyfish Search–Gradient Based Optimizer (JS–GBO) is proposed to optimize the exergo-economic performance of an Al_2O_3/water PV/T–TEG system for constrained optimization. To overcome these issues, a hybrid Jellyfish Search–Gradient Based Optimizer (JS–GBO) is proposed for constrained exergo-economic optimization of an Al_2O_3/water PV/T–TEG system. A steady-state thermal, hydraulic, exergy, and economic model is developed, and a large search is carried out by the Jellyfish Search phase, while a local search is carried out by the implemented Gradient Based Optimizer phase. The model is tested with 366 daily weather records from the station of Baghdad during the year 2020 and is compared with JS, GBO, GA, and PSO with the same budget of the evaluation process. A feasible JS–GBO design is obtained at 0.04611 kg s^{-1} mass flow rate, 9.7906 m^2 collector area, 32.783 °C TEG hot-side temperature, and 0.3397 vol.% nanoparticle concentration. An exergy efficiency of 17.5507%, net electrical power of 1468.47 W, useful thermal output of 3374.44 W, NPV of 1180.78 USD, and LCOE of 0.07932 USD kWh^{-1} are obtained. The pressure drop and energy balance conditions are fulfilled. Based on the best mean objective and lowest variability, PSO is determined as the feasible and competitive, if not the best, method when compared to JS–GBO

DOI: https://doi.org/10.54660/.IJMRGE.2026.7.6.231-246

Keywords: Exergo-economic optimization, Jellyfish Search, Nanofluid, PV/T–TEG system, Renewable energy

1. Introduction

The rising demand for electricity, coupled with worries about fossil-fuel usage, energy security and emissions of greenhouse gases, has grown the deployment of renewable-energy technologies. Solar energy is a renewable energy source which is widely acknowledged due to its distribution capability, modularity, and availability. Photovoltaic (PV) systems are therefore widely used to directly transform the solar irradiation into electricity [1]. A significant portion of the solar radiation is, however, absorbed as heat and not electricity. This temperature increase results in a decrease in the efficiency of the PV-cell to convert electricity. Thus, it is necessary to have efficient thermal management to preserve the PV performance and collection of the rejected heat for beneficial purposes [2].

To overcome this limitation, a new technology that generates both useful thermal energy and electricity is developed, known as photovoltaic/thermal (PV/T) collectors. A typical PV/T involves a working fluid being circulated through a thermal absorber mounted on the back of the PV module [3]. The heat is removed from the photovoltaic cells, the temperature of the photovoltaic cell is lowered, and the thermal energy is supplied for the use of domestic, industrial or low-temperature heating. These benefits notwithstanding, the overall performance of a PV/T system is still highly sensitive to the thermal characteristics of the coolant, the solar irradiance, ambient conditions, mass-flow rate, collector shape and operating temperature [4]. Furthermore, it is not always the most economical system that will result from improved thermal output since the additional pumping power or the cost of materials or the number of additional component parts required could compensate for the energy gain [5].

In hybrid solar system, another possibility of energy recovery is through the use of thermoelectric generators (TEGs) [6]. A TEG is a device that converts directly a temperature difference to electricity using the Seebeck effect. A hot side of the TEG can be thermally connected to the absorber or the rear surface of the PV, and the cold side can be cooled by the circulating fluid, when being integrated with a PV/T collector [7]. Under this scheme, a fraction of the thermal energy produced is used to generate additional electricity. However, the temperature difference between the module, thermal-contact resistance, cooling efficiency and material properties have significant influence on TEG performance. Inappropriate operating conditions may lead to sub-optimal electrical gain and undesirable thermal loss or extra costs to the system [8].

Nanofluids are being given more and more attention as enhanced heat-transfer fluids for use in solar thermal and PV/T systems. These fluids are made by suspending metallic, metal-oxide, carbon or hybrid nanoparticles in a traditional base fluid like water, ethylene glycol or a water-glycol base fluid [9]. Better heat removal from the PV cells can be achieved due to the increase of thermal conductivity and convective heat transfer properties of the cell [10]. This will lead to lower PV operating temperatures, higher thermal output, and better TEG temperature gradients. But the concentration of the nanoparticles in the nanofluid needs to be carefully chosen as high nanoparticle loading may lead to higher pumping-power requirement, higher pressure drop, higher fluid preparation cost, and higher viscosity [11]. This means that when using nanofluids a multi-variable design problem arises, where the thermal penalty has to be weighed against the hydraulic and economic penalties [12].

Energy efficiency should not be the sole criterion for assessing the performance of an integrated PV/T–TEG system [13]. An analysis of energy tells us how much useful energy is produced, while an exergy analysis tells us how good the thermodynamic quality of the energy is and what useful work it could [13, 14]. Moreover, the system's practicality is verified with economic metrics such as capital investment, operation and maintenance cost, levelized cost of energy, payback period and return on investment [15]. Therefore, a framework that combines thermodynamic performance and cost-related consequences is necessary, known as an exergo-economic framework. Such a system enables identification of the operating conditions for the technically efficient and economically viable hybrid solar-energy system [16].

The optimization of this system is difficult, due to the non-linear interaction between some of its decision variables [17]. The mass-flow rate of the coolant influences heat removal, pumping power, PV temperature, and TEG cooling conditions. The collector area influences solar-energy collection as well as installation costs [3, 18]. The temperature on the hot side of the TEG has a significant effect on the temperature gradient that can be achieved and on the electrical output, while the concentration of the nanofluid has a significant effect on heat-transfer enhancement and hydraulic losses [7-10, 19]. When the objective function is complex, nonlinear, constrained, and multiple modes, conventional optimization methods might be less applicable. For this reason, metaheuristic algorithms are very popular and can be used to achieve global search without making restrictive assumptions on the mathematical structure of the objective function [20, 21].

A hybrid Jellyfish Search–Gradient Boosting Optimizer (JS–GBO) framework for the exergo-economic optimization of a PV/T system integrated with thermoelectric generators using a nanofluid is proposed in this work. The population-based movement mechanism of the Jellyfish Search algorithm guides the search process to explore the search space broadly using the algorithm Jellyfish Search [22]. The Gradient Boosting Optimizer is then used to further optimize the most potential solutions and local exploitation. A search process which is both reliable and effective is desired by utilizing both exploration and exploitation mechanisms. The exergo-economic performance of the proposed hybrid system is optimized by using the integrated framework by selecting the optimized operating and design variables [23].

The combination of PV/T, thermoelectric generation, nanofluids and optimization is an unresolved design challenge, but each has been studied in the past [1, 3, 6]. Coupled thermal, hydraulic, electrical and economic effects affect the electrical and thermal performance of a PV/T-TEG system [7, 8]. For instance, higher heat transfer performance from the nanofluid can be utilized for the cooling of PV systems as well as the TEG power generation systems, but may also increase pumping needs and operating costs [3, 9, 11]. Thus, optimization needs to be done in a coordinated way to determine the optimal combination of flow rate, collector area, TEG hot-side temperature, and nanofluid concentration due to technical and economic constraints [17, 20].

The main objective of this study is to develop and apply a hybrid JS–GBO optimization framework for a nanofluid-based PV/T–TEG system. In particular, the following objectives will be tackled:

- To develop the thermal, electrical, exergy and economic models of the integrated PV/T–TEG system.
- To investigate the effect of nanofluid concentration on improving heat transfer, the reduction in PV temperature, TEG output, and pumping-power demand.
- To design an exergo-economic objective function that incorporates the energy quality and the economic viability.
- To maximize the flow rate of the coolant, the collector area, hot-side temperature of the TEG, and the concentration of the nanofluid under certain operating conditions.
- To compare the proposed JS–GBO framework with the stand-alone JS, GBO, genetic algorithm and particle swarm optimization methods.

The main contributions of this paper are summarized as follows:

- A complete exergo-economic model of PV/T collector with thermoelectric generators using nanofluids is developed.
- The synergic effects of the nanofluid heat-transfer improvement, hydraulic losses, PV electrical performance, thermal recovery, and TEG power generation are taken into account in a single optimization framework.
- A hybrid Jellyfish Search–Gradient Boosting Optimizer is proposed to achieve the balance between global exploration and local exploitation in the system-design process.
- The proposed method is aimed at optimizing simultaneously the main operating and design variables instead of separately optimizing the energy and economic indicators.
- A comparative assessment is carried out with the individual and conventional optimization algorithms, according to the convergence behavior, the optimum value of the objective function, the energy indicators, the exergy indicators, and the economic parameters.

The rest of this paper is organized in the following manner. In Section 2, the nanosecond based PV/T–TEG configuration is described and the literature is reviewed. In Section 3, the energy, exergy and economic formulations are presented, followed by the proposed optimization framework JS–GBO, decision variables and constraints. The optimization results, comparative algorithmic performance, sensitivity analysis, energy and exergy outcomes and economic indicators are presented and discussed in Section 4. Finally, in Section 5, the main conclusions, practical implications, limitations and recommendations for future work are presented.

2. System Description and Literature Review

2.1 PV/T System Architecture

A photovoltaic/thermal (PV/T) system is configured to generate electrical and thermal energy from the same incident solar radiation. In general, the hybrid collector is built of a PV module, a transparent protective cover, encapsulating layers, a thermal absorber plate, coolant channels, thermal insulation and supporting structural elements. A fraction of the sunlight is absorbed by the PV cells and generates electricity [1]. The energy left over is mostly converted to heat, causing the cell's temperature to rise, and lowering electrical efficiency. Hence, a coolant channel is located behind the PV module or absorber plate to dissipate the excess heat and keep the operating temperature more desirable [3].

The proposed configuration is such that a nanofluid is circulated in the cooling channel. The heat is transferred from PV cells to the absorber plate, and then to the circulating nanofluid [3]. The heat recovered is then ready for low temperature thermal uses or for additional recovery by a thermoelectric generator. The electrical power generated by the PV module is influenced by the solar irradiance, cell temperature, electrical properties and surface conditions [6]. In the meantime, the useful thermal production is controlled by the fluid mass-flow rate, inlet temperature, channel design, area of the collector and the thermophysical properties of the fluid. A PV/T collector is thus not considered as a standalone PV module, but more of a PV/electrical–thermal energy-conversion system. Research on the PV/T–TEG systems with the use of nanofluids shows that the output of the PV can be enhanced with effective cooling, and the recovered thermal energy can be utilized elsewhere [7].

The detailed configuration of the modeled nanofluid based PV/T–TEG system is shown in Fig. 1. Covered PV layer receives solar radiation and a fraction of the absorbed energy is utilized for generating electricity while the rest is conducted toward the absorber and TEG modules [6], [8]. The TEG array is used for converting some of the temperature difference into extra electrical power, and the circulating Al_2O_3/water nanofluid is employed to remove heat from the absorber and the cold side of the TEG. The convective, radiative, back-side, optical and hydraulic losses are accounted for in the system balance while the recovered heat is provided as a useful thermal output [14]. The electrical, thermal, hydraulic, exergy and economic outputs are then given to the exergo-economic assessment [15].

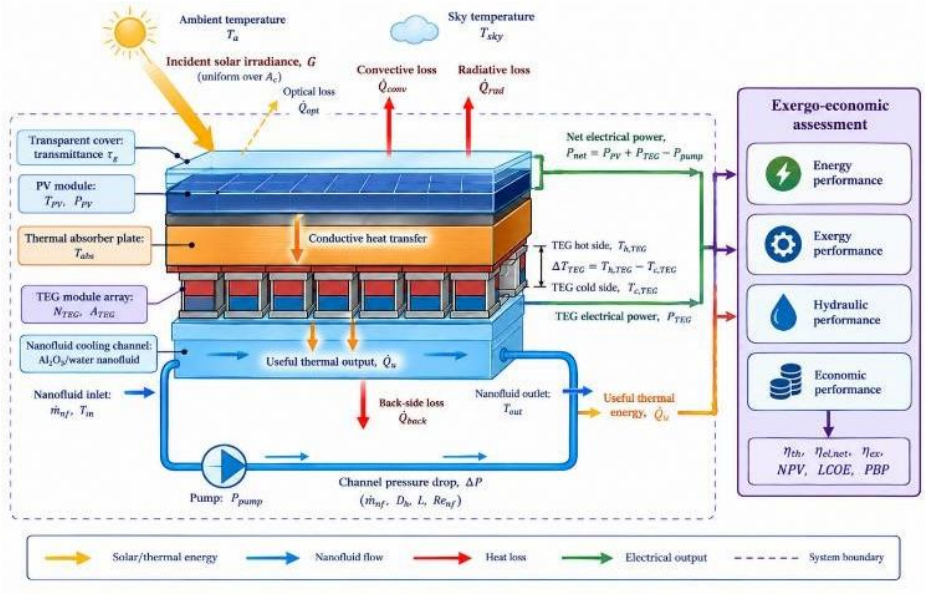


Fig 1: Detailed schematic of the nanofluid-based PV/T collector integrated with thermoelectric generators, including the principal energy, fluid-flow, electrical, and heat-loss pathways.

2.2 Thermoelectric Generator Integration

A voltage is produced if there is a temperature difference between two sides of a thermoelectric module. Typically a module consists of thermoelectric legs of p-type and n-type semiconductor materials. PV/T-TEG system, the hot side of the TEG is thermally coupled to the heated collector surface, absorber plate or rear surface of the PV module. The coolant channel or auxiliary heat sink is connected to the cold side. Therefore, part of the waste heat which is not directly transformed by the PV module is used for producing additional electrical power [6, 7].

The TEG performance depends on the difference between the hot and cold side temperature, the contact resistance, module geometry, thermal conductivity, electrical resistance and cooling conditions. Increased difference between the two temperatures can enhance the value of TEG voltage and output power, but too high temperature can speed up PV degradation and can cause thermal loss. As such, a balance is needed between PV cooling and useful heat extraction, and TEG operation. The numerical analysis results indicate that the temperature on the cold-side of the system will be lowered and the TEG output will be increased when using the nanofluid to cool, but the system performance is still sensitive to the coolant conditions and channel geometry [3, 7, 8].

2.3 Nanofluid Cooling Medium

Nanofluids are simply a traditional base fluid, like water, ethylene glycol or a water–glycol mixture, which is mixed with nanoparticles. Improving the thermo-physical properties of the cooling fluid can be achieved by the use of metallic, metal oxide, carbon and hybrid nanoparticles. A number of nanoparticles, such as aluminum oxide, copper oxide, titanium dioxide, silica, graphene and hybrid versions thereof, are generally considered. An appropriate choice of the type, size, morphology and volume concentration of the nanoparticles generally leads to improved effective thermal conductivity and convective heat-transfer performance [3, 9, 10].

The heat transfer ability of the nanofluids is greater than that of the conventional fluids so more heat can be removed from the PV module. Thus, PV cell temperature can be lowered, thermal generation can be raised and the temperature difference over the TEG can be optimized. However, the practical implications of using nanofluids with the associated practical trade-offs must be taken into account. Increasing the concentration of nanoparticles may result in a decrease in viscosity and pressure and increase the pumping power needed. Other factors such as nanoparticle agglomeration, sedimentation, corrosion, long-term stability, and preparation cost and maintenance should also be taken into consideration. Although the performance of hybrid nanofluids could yield better energy, exergy, environmental and economic performance in simulated PV/T–TEG systems, the feasibility of the hybrid nanofluids is dependent on the operating conditions and cost parameters [4, 11, 12].

2.4 Current Optimization Methods and Techniques

The existing PV/T and PV/T–TEG studies are mostly experimental tests, numerical simulation, parametric analysis, thermodynamic modeling, and optimization-based design. The performance of the system is evaluated in experimental studies under controlled indoor conditions or under outdoor solar conditions. Common measured parameters include electrical power, thermal output, PV surface temperature, fluid outlet temperature, pressure drop and TEG voltage. While experiment is crucial, it is often limited by prototype costs, measurement uncertainty, seasonal variation, and the number of operating conditions that can be subjected to experiments [1, 4].

Current Optimization Methods and Techniques, D. 24th February 2014.Optimum techniques and methods: current, D., Feb. 24, 2014. Most of the existing PV/T and PV/T–TEG studies involve experimental testing or numerical simulation, parametric analysis, and thermodynamic modeling and optimization-based design. Experimental studies are conducted in the system, either in controlled indoor environment or in solar outdoor environment, to measure the system performance. Common parameters are measured are electrical power, thermal power output, PV surface temperature, fluid outlet temperature, pressure drop and TEG voltage. Experimental testing is crucial but the prototype is expensive, the measurement is uncertain and the tests are limited in number of operating conditions and seasonal variations [1, 4].

Numerical methods are often employed to simulate temperature distribution, flow of fluids, thermal resistance, electrical output and exergy performance. CFD, FE and thermal-resistance models are used to study the cooling-channel designs, the placement of TEGs, heat transfer characteristics and behavior of nanofluids. There is also a wide use of parametric analysis in which the other variables are fixed while one variable is varied. This method offers physical insight, but does not always fully reflect interactions between flow rate, concentration of nanoparticles, collector area, and the temperature of the TEG. Assessment of the literature indicates that most of the available PV/T-TEG nanofluid literature is still numerical or theoretical, and there are relatively few experimental studies and three-dimensional coupled models [3, 9].

Non-linear and constrained operating conditions are addressed using metaheuristic optimization techniques to enhance PV/T performance. A set of candidate solutions are evolved using a genetic algorithm (GA) which consists of selection, crossover and mutation. The candidate solutions are updated based on particle's own and swarm's search experience by the particle swarm optimization (PSO). Other nature inspired approaches are also used for optimizing the exergy efficiency, electrical output, multi objective performance indicators, and cost, as well as for thermal efficiency. Algorithms, however, must converge; they must not converge too quickly; one must be able to select parameters that are suitable; and they must be performing well when there is a good balance between exploration and exploitation [17, 20, 22, 23].

Optimization for integrated PV/T–TEG systems is commonly performed on exergy efficiency, electrical power, or the thermal performance, or economic indicators. This can result in a solution which is good for one measure, but bad for the system as a whole. A high mass-flow rate, for instance, may enhance the PV cooling performance, but may also raise the pumping power and the operational expenses. Similarly, high nanoparticle concentrations can improve heat transfer performance, but can also result in higher viscosity, higher pressure drop and higher nanofluid cost. So, it is necessary to perform simultaneous exergo-economic optimization to determine a design which can give an optimum balance between thermodynamic quality and economic viability. Table 1 introduces the problems and limitations of current

methods [13, 15, 17].

2.5 Research Gap

The available studies have shown that PV/T systems can be enhanced by implementing the process of liquid cooling, circulation of nanofluid, modification of the thermal channel, and the process of extraction of waste heat using the TEG. The TEG is a component used to recover some of the cooling energy and convert it to further electricity generation, and enhanced cooling is generally correlated with the reduction of the PV temperature and an increased electrical performance. These improvements are not, however, always considered at the same time in terms of thermodynamics and economy. The extra cost and hydraulic penalties of circulation of the nanofluid are often not fully accounted for in electrical, thermal and exergy performance indicators [3, 9, 11, 13].

Moreover, the study of PV/T combination is mostly conducted independently for optimization of PV/T module, TEG module, cooling channels or nanofluid properties. While the conventional and metaheuristic optimization methods have been used for related energy systems, there is still a lack of study on the integrated application of the hybrid Jellyfish Search and Gradient Boosting Optimizer (GBO) algorithms to a PV/T–TEG system using a nanofluid as an absorber. The problem is filled by the proposed study that integrates the global exploration ability of the Jellyfish Search algorithm with the refined exploitation ability of the Gradient Boosting Optimizer. Thus, a single exergo-economic objective function is optimized, as well as simultaneous thermal, electrical, hydraulic, and cost constraints are taken into account [17, 20, 22, 23].

Table 1: Problems and Limitations of Current Methods

No	Current method or application	Main application in PV/T–TEG systems	Problems and limitations
1.	Conventional PV cooling	PV temperature reduction using air or water cooling	Limited heat-transfer capability may be obtained, particularly under high solar irradiance. Water cooling can require significant flow rates and pumping energy.
2.	Air-based PV/T collectors	Heat removal and low-complexity thermal recovery	Lower heat capacity and heat-transfer coefficient are generally provided compared with liquid cooling. Larger ducts or fans may be required.
3.	Water-based PV/T collectors	PV cooling and useful thermal-energy recovery	Corrosion, leakage, freezing risk, scaling, and pumping-power consumption can be introduced. Heat-transfer enhancement is limited by the base-fluid properties.
4.	Nanofluid cooling	Enhanced heat transfer and reduction of PV operating temperature	Increased viscosity, pressure drop, pumping power, sedimentation, nanoparticle agglomeration, stability concerns, and preparation cost can be introduced.
5.	TEG integration with PV or PV/T	Recovery of waste heat as supplementary electricity	TEG efficiency is relatively low when the temperature difference is small. Thermal-contact resistance and inadequate cold-side cooling can reduce the generated power.
6.	Parametric analysis	Evaluation of the effect of one variable at a time	Coupled interactions among variables are not fully represented. A global optimal solution is not guaranteed.
7.	Experimental testing	Prototype validation and real-condition performance measurement	High cost, long test duration, weather dependence, sensor uncertainty, and restricted operating conditions limit broad design exploration.
8.	CFD and finite-element simulation	Temperature, flow, and thermal-stress prediction	High computational time can be required. Accurate results depend on boundary conditions, property correlations, and model assumptions.
9.	Genetic algorithm	Global search for design and operating variables	Premature convergence may occur, and performance can be sensitive to population size, crossover rate, mutation rate, and stopping criteria.
10.	Particle swarm optimization	Fast optimization of nonlinear design variables	Local optima can trap the swarm, particularly when diversity is reduced during later iterations.
11.	Single-objective optimization	Maximization of power, efficiency, or exergy separately	Economic cost, pumping power, material cost, and long-term feasibility may be neglected. A technically optimal design may not be economically optimal.
12.	Separate PV/T and TEG optimization	Independent enhancement of PV/T cooling or TEG operation	Thermal coupling between the PV module, coolant, and TEG is not fully exploited. The integrated system-level optimum may be missed.

3. Proposed Methodology

3.1 Model formulation and decision variables

In the present study, a numerical, steady-state exergo-economic model of a PVT system with thermoelectric generator modules coupled with a nanofluid-cooled PV system is developed. The model is run at a given ambient temperature, and solar irradiance. It is assumed that the collector is uniformly irradiated and the heat transfer processes at the collector surface can be represented as a lumped one-dimensional thermal network. The temperature field is iteratively calculated until the maximum difference between the calculated temperature at the nodes is less than the numerical tolerance specified. The decision vector is a vector of zeros and ones that can be used to characterize a decision as (1):

$$x = \left[\dot{m}_{nf},\ A_c,\ T_{h,TEG},\ \phi\right]^T, \quad (1)$$

The nanofluid mass-flow rate is denoted as $\dot{m}_{nf}$, the collector area is denoted as A_c, the prescribed TEG hot-side temperature is denoted as $T_{h,TEG}$, and the volume

concentration of nanoparticles is denoted as ϕ. The optimization is performed for an Al_2O_3/water nanofluid. For the numerical implementation, the following bounds of the decision variables are employed. Table 2 introduces rang of the independent variable used in the model [13, 15].

Table 2: Ranges of the Independent Variables Used in the Model

Variable	Lower bound	Upper bound	Unit
Nanofluid mass flow rate ($\dot{m}_{nf}$)	0.005	0.100	kg s^{-1}
Collector area (A_c)	1	10	m^2
Hot side temperature of TEG ($T_{h,TEG}$)	25	80	°C
Nanoparticle volume fraction (ϕ)	0.0033	0.0300	volume fraction

The objective function is an exergoeconomic index with weights. All of its exergy, economic and cost terms are normalized with respect to a solution-independent minimum–maximum normalization instead of a solution-dependent minimum–maximum normalization. This formulation allows to give the objective scale without changing it during the optimization process.

The computational flow of the proposed exergo-economic optimization methodology is given in Fig. 2. Initially, the decision variables are given the bounds of the problem constraints and then each candidate solution is to be tested through the coupled thermal, TEG, hydraulic, exergy, and economic models for the problem. Norm and penalize constraint violations and retain improved feasible candidates. The Jellyfish Search phase is then applied for general global exploration and the highest-ranking JS individuals are passed to a complete GBO population to be refined locally.

Feedback is given by repeatedly evaluating the model, comparing the model to an objective or checking the constraint(s) and updating the best model solution until the iteration and independent run limits are met. The final possible design is then checked using the energy-balance residual and annual equivalent-operating-hours simulation [22, 23].

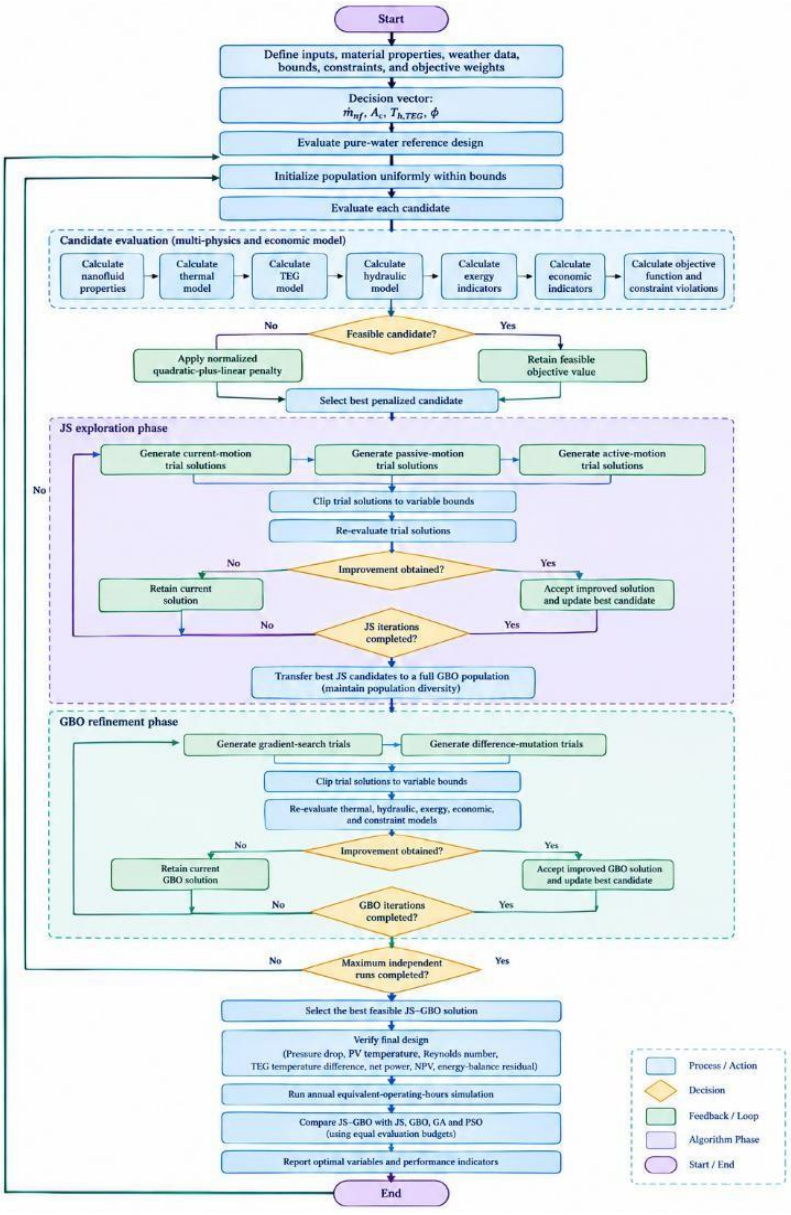


Fig 2: Flowchart of the proposed JS–GBO-based exergo-economic optimization methodology.

3.2 Energy and thermal model

The amount of solar-energy that the collector receives from the incident sun is as (2):

$$\dot{Q}_{solar} = GA_c, \quad (2)$$

where G is the design-point solar irradiance. The amount of solar energy absorbed by PV-cell region and exposed absorber region is computed as (3), (4):

$$S_{PV} = \tau_g \alpha_{PV} PF\, GA_c, \quad (3)$$

$$S_{abs} = \tau_g \alpha_{abs}(1 - PF) GA_c, \quad (4)$$

where τ_g is the cover transmittance, α_{PV} and α_{abs} are the absorptivity's of the PV and absorber regions, respectively, and PF is the PV packing factor. The remaining optical loss is as (5):

$$\dot{Q}_{opt} = \dot{Q}_{solar} - S_{PV} - S_{abs}. \quad (5)$$

The PV electrical efficiency is a function of the PV cell temperature as given by (6):

$$\eta_{PV} = \eta_{ref}\left[1 - \beta_{PV}\left(T_{PV} - T_{ref}\right)\right], \quad (6)$$

where η_{ref} is the reference efficiency, β_{PV} is the temperature coefficient (expressed as a positive value), and T_{ref} is the reference temperature. The PV input absorbed by the PV region is used to calculate the electrical power generated by this region as (7):

$$P_{PV} = \eta_{PV} \frac{S_{PV}}{\alpha_{PV}}. \quad (7)$$

The convective loss on the wind-side is determined as (8):

$$\dot{Q}_{conv} = h_w A_c (T_{PV} - T_a), \quad (8)$$

where;

$$h_w = 5.7 + 3.8 V_w. \quad (9)$$

In this case, V_w is the wind speed and T_a is is the ambient temperature. A Swinbank-type relationship is used to estimate the effective sky temperature as (10):

$$T_{sky,K} = 0.0552\, T_{a,K}^{1.5}, \quad (10)$$

where the subscript K means, absolute temperature in kelvin. The radiative loss is then affected by this. This therefore affects the radiative loss as (11):

$$\dot{Q}_{rad} = \varepsilon \sigma A_c\left[(T_{PV} + 273.15)^4 - T_{sky,K}^4\right], \quad (11)$$

whereas, ε is surface emissivity and σ is Stefan–Boltzmann constant. The heat loss from back-side is

$$\dot{Q}_{back} = U_b A_c (T_{abs} - T_a), \quad (12)$$

where U_b is the back-loss coefficient and T_{abs} is the absorber temperature. Thus, the total thermal loss is as (13):

$$\dot{Q}_{loss} = \dot{Q}_{conv} + \dot{Q}_{rad} + \dot{Q}_{back}. \quad (13)$$

A coupled two-node thermal balance is used to obtain the PV and absorber temperatures. The PV balance is depicted by (14):

$$S_{PV} - P_{PV} = \dot{Q}_{conv} + \dot{Q}_{rad} + K_{pa}(T_{PV} - T_{abs}), \quad (14)$$

A material that absorbs the radiation is indicated by (15):

$$S_{abs} + K_{pa}(T_{PV} - T_{abs}) = \dot{Q}_{back} + UA_f\left(T_{abs} - T_f\right) + \dot{Q}_{TEG,h}, \quad (15)$$

where $K_{pa} = A_c / R_{pa}$ is the PV-to-absorber conductance, R_{pa} is is the effective PV-to-absorber thermal resistance, T_f is the mean temperature. The nanofluid temperature is denoted as nanofluid temperature and UA_f is the absorber to fluid conductance. The useful heat transferred to the nanofluid is calculated from the calculated conductance and the difference in temperature, which is determined as (16):

$$\dot{Q}_u = UA_f \max\left(T_{abs} - T_f, 0\right) + \dot{Q}_{TEG,c}, \quad (16)$$

where $\dot{Q}_{TEG,c}$ is the heat rejected from cold side of the TEG to the nanofluid. The temperature of the outlet gas is measured as (17):

$$T_{out} = T_{in} + \frac{\dot{Q}_u}{\dot{m}_{nf} c_{p,nf}}, \quad (17)$$

subject to upper bound number of the implementation Let $T_{in} = T_a + \Delta T_{in}$, where $\Delta T_{in} = 2$ °C denote the inlet temperature. The efficiency of the heat transfer system is as (18):

$$\eta_{th} = \frac{\dot{Q}_u}{GA_c}. \quad (18)$$

The relative energy-balance residual used to verify the numerical solution is as (19):

$$RE = \frac{\dot{Q}_{solar} - (\dot{Q}_{opt} + P_{PV} + \dot{Q}_u + \dot{Q}_{conv} + \dot{Q}_{rad} + \dot{Q}_{back} + P_{TEG})}{\dot{Q}_{solar}}. \quad (19)$$

A small value of $|RE|$ indicates numerical consistency of the thermal model [1].

3.3 Thermoelectric generator model

Each module represents a certain fraction of the collector area and makes up the TEG array [6], [7]. The number of installed modules is equal to (20):

$$N_{TEG} = \max\left(1, \left\lfloor \frac{f_{cover} A_c}{A_{mod}} \right\rfloor\right), \quad (20)$$

The fraction of TEG coverage f_{cover} is the ratio of area of the cover to the area of one module A_{mod}. The effective Hot Side conductance is given by (21):

$$K_h = \frac{1}{R_h/N_{TEG}}. \quad (21)$$

The TEG is only turned on if the temperature of the absorber is above the set hot-side temperature. Thus,

$$\dot{Q}_{TEG,h} = K_h \max\left(T_{abs} - T_{h,TEG}, 0\right). \quad (22)$$

The cold-side temperature is the result of the heat rejected by the TEG and the greater cold-side heat transfer conductance as (23):

$$T_{c,TEG} = T_{in} + \frac{\dot{Q}_{TEG,c}}{h_{c,TEG}A_{TEG}}. \quad (23)$$

The electrical model's temperature difference is as (24):

$$\Delta T_{TEG} = \max\left(T_{h,TEG} - T_{c,TEG}, 0\right). \quad (24)$$

The TEG power is calculated as (25):

$$P_{TEG,raw} = N_{TEG}\frac{\left(N_p \alpha_{TEG}\Delta T_{TEG}\right)^2}{4R_{int}}, \quad (25)$$

where N_p is the number of thermocouple pairs per module, α_{TEG} is the Seebeck coefficient and R_{int} is the internal resistance. In order to preserve the thermal balance, the power generated is limited dependent on the hot-side heat available as (26):

$$P_{TEG} = \min\left(P_{TEG,raw}, \dot{Q}_{TEG,h}\right). \quad (26)$$

The heat that needs to be rejected to the coolant is then as (27):

$$\dot{Q}_{TEG,c} = \max\left(\dot{Q}_{TEG,h} - P_{TEG}, 0\right). \quad (27)$$

The gross and net electrical power are as (28), (29):

$$P_{gross} = P_{PV} + P_{TEG}, \quad (28)$$

$$P_{net} = P_{PV} + P_{TEG} - P_{pump}. \quad (29)$$

Accordingly,

$$\eta_{el,net} = \frac{P_{net}}{GA_c}, \quad \eta_{en,overall} = \frac{P_{net}+\dot{Q}_u}{GA_c}. \quad (30)$$

3.4 Hydraulic model and nanofluid properties

The mixture relation is used for the calculation of the nanofluid density as (31) [3]:

$$\rho_{nf} = (1-\phi)\rho_f + \phi\rho_p. \quad (31)$$

The volumetric heat capacity and specific heat are as (32), (33):

$$\left(\rho c_p\right)_{nf} = (1-\phi)\left(\rho c_p\right)_f + \phi\left(\rho c_p\right)_p, \quad (32)$$

$$c_{p,nf} = \frac{\left(\rho c_p\right)_{nf}}{\rho_{nf}}. \quad (33)$$

Brinkman relation is used to estimate the dynamic viscosity as (34):

$$\mu_{nf} = \frac{\mu_{bf}(T_f)}{(1-\phi)^{2.5}}, \quad (34)$$

where viscosity of base-fluid has been determined as a function of temperature. The Maxwell model is used to determine the effective thermal conductivity as (35):

$$k_{nf} = k_{bf}\left(T_f\right)\frac{k_p+2k_{bf}+2\phi\left(k_p-k_{bf}\right)}{k_p+2k_{bf}-\phi\left(k_p-k_{bf}\right)}. \quad (35)$$

The Prandtl number is as (36):

$$Pr_{nf} = \frac{\mu_{nf}c_{p,nf}}{k_{nf}}. \quad (36)$$

The mean velocity and the flow cross sectional area are as (37):

$$A_f = \frac{\pi D_h^2}{4}, \quad u_{nf} = \frac{\dot{m}_{nf}}{\rho_{nf}A_f}. \quad (37)$$

The Reynolds number is as (38):

$$Re_{nf} = \frac{\rho_{nf}v_{nf}D_h}{\mu_{nf}}. \quad (38)$$

The implementation is based on the following correlations for the case of laminar, transitional and turbulent flow. When the flow is laminar $Nu = 4.36$ and $f = 64/Re_{nf}$. The values for the transitional range are computed as fixed values at $Re = 4000$. These Dittus–Boelter and Blasius correlations are used for turbulent flow as (39) [4, 9]:

$$Nu = 0.023Re^{0.8}Pr^{0.4}, \quad f = 0.3164Re^{-0.25}. \quad (39)$$

The heat-transfer coefficient for the fluid side is as (40):

$$h_f = \frac{Nu\,k_{nf}}{D_h}. \quad (40)$$

The length of the fluid-filled channel is the pitch times the number of absorbers $L = A_c/pitch$ as (41):

$$UA_f = F_{bond}h_f(\pi D_h L), \quad (41)$$

where F_{bond} is the bond or fin efficiency. The losses of distributed or minor flows are included in the pressure drop as (42):

$$\Delta P = f\frac{L}{D_h}\frac{\rho_{nf}v_{nf}^2}{2} + K_{minor}\frac{\rho_{nf}v_{nf}^2}{2}. \quad (42)$$

The volumetric flow rate and the pumping power are as (43):

$$\dot{V}_{nf} = \frac{\dot{m}_{nf}}{\rho_{nf}}, \quad P_{pump} = \frac{\Delta P \dot{V}_{nf}}{\eta_{pump}}. \tag{43}$$

3.5 Exergy and economic calculations

The exergy rate of the sun is determined with the Petela expression as (44):

$$\dot{E}x_{solar} = GA_c\left[1 - \frac{4}{3}\left(\frac{T_{a,K}}{T_s}\right) + \frac{1}{3}\left(\frac{T_{a,K}}{T_s}\right)^4\right], \tag{44}$$

where T_s is is the effective temperature of the solar-source. Net electrical power is equal to electrical exergy as (45):

$$\dot{E}x_{el} = P_{net}. \tag{45}$$

The thermal exergy available is as (46):

$$\dot{E}x_{th} = \max\{\dot{m}_{nf}c_{p,nf}\left[\left(T_{out,K} - T_{in,K}\right) - T_{a,K}\ln\left(\frac{T_{out,K}}{T_{in,K}}\right)\right], 0\}. \tag{46}$$

Net useful exergy and exergy efficiency are therefore;

$$\dot{E}x_{net} = P_{net} + \dot{E}x_{th}, \quad \eta_{ex} = \frac{\dot{E}x_{net}}{\dot{E}x_{solar}}. \tag{47}$$

The rate of exergy destruction, or the rate of exergy loss as (48):

$$\dot{E}x_{dest} = \dot{E}x_{solar} - \dot{E}x_{net}. \tag{48}$$

The capital costs consist of PV, absorber, TEG, nanofluid, pump and BOS components as (49):

$$C_{inv} = C_{PV} + C_{abs} + C_{TEG} + C_{nf} + C_{BOS}, \tag{49}$$

with

$$\begin{aligned} C_{PV} &= c_{PV}A_c, \\ C_{abs} &= c_{abs}A_c, \\ C_{TEG} &= c_{TEG}N_{TEG}. \end{aligned} \tag{50}$$

The cost of the nanofluid is determined by analysing the mass fraction of the nanoparticles.

$$w_{np} = \frac{\phi\rho_p}{\rho_{nf}}, \tag{51}$$

so that

$$C_{nf} = m_{nf}\left[\left(1 - w_{np}\right)c_{bf} + w_{np}c_{np}\right]. \tag{52}$$

The annual operation and maintenance cost, the cost of pumping-energy and the annual amount of pumping-energies are as (53), (54), (55):

$$C_{OM} = f_{OM}C_{inv}, \tag{53}$$

$$C_{pump,ann} = P_{pump}H_{eq}c_e, \tag{54}$$

$$\begin{aligned} E_{net,ann} &= P_{net}H_{eq}/1000, \\ E_{th,ann} &= \dot{Q}_u H_{eq}/1000, \end{aligned} \tag{55}$$

where H_{eq} is the equivalent annual operating duration in hours. Revenue earned from electricity and useful-heat are as (56):

$$R_{el} = E_{net,ann}c_e, \quad R_{th} = E_{th,ann}c_{th}. \tag{56}$$

The cash flow of each year is as (57):

$$CF = R_{el} + R_{th} - C_{OM} - C_{pump,ann}. \tag{57}$$

The NPV of the project over its lifetime of N years with a discount rate of r is as (58):

$$NPV = -C_{inv} + CF\sum_{y=1}^{N}\frac{1}{(1+r)^y}. \tag{58}$$

The factor for the recovery of the capital is as (59):

$$CRF = \frac{r(1+r)^N}{(1+r)^N - 1}, \tag{59}$$

The annualized capital cost is $C_{ann} = CRF\, C_{inv}$. The code employs the following net levelized electricity cost approach, which includes the credit for useful-heat revenue as (60):

$$LCOE_{net} = \frac{C_{ann} + C_{OM} + C_{pump,ann} - R_{th}}{\max(E_{net,ann}, \epsilon)}. \tag{60}$$

Simple payback period is as (61):

$$PBP = \frac{C_{inv}}{\max(CF, \epsilon)}, \tag{61}$$

and the reported return indicator is the NPV to investment ratio as (62):

$$ROI_{NPV} = \frac{NPV}{C_{inv}}. \tag{62}$$

This definition is used in the code and should not be confused with an annual cash-flow return ratio.

3.6 Weighted exergo-economic objective and constraints

The objective terms are re-scaled with reference to the pure-water design as (63) [13], [15], [17]:

$$\begin{aligned} I_{ex} &= \frac{\eta_{ex}}{\eta_{ex,ref}}, \\ I_{econ} &= \frac{NPV}{NPV_{ref}}, \\ I_{cost} &= \frac{LCOE_{net}}{LCOE_{ref}}. \end{aligned} \tag{63}$$

The objective for the weighted maximization is as (64):

$$F = w_1 I_{ex} + w_2 I_{econ} - w_3 I_{cost}, \tag{64}$$

where;

$$w_1 + w_2 + w_3 = 1 \tag{65}$$

Minimization of the penalized objective by the optimization routine as (66):

$$J = -F + P_{pen}. \tag{66}$$

The constraints that have been implemented are as (67), (68), (69), (70), (71):

$$T_{PV} \leq 85\ °C, \quad (67)$$
$$\Delta T_{TEG} \geq 5\ K, \quad (68)$$
$$Re_{nf} \leq 10{,}000, \quad (69)$$
$$\Delta P \leq 47{,}500\ Pa, \quad (70)$$
$$P_{net} > 0,\ NPV > 0,\ T_{h,TEG} \leq T_{abs}. \quad (71)$$

The pressure-drop limit is 47.5kPa, which is five percent below the physical limit of 50kPa. The limits of the constraint violations are normalized and the violations are penalized with a large quadratic-plus-linear penalty. A candidate is feasible if all the normalized violations are within numerical tolerance.

3.7 Jellyfish Search, GBO, and hybrid implementation

Initial population is set at random in between the bounds. The Jellyfish Search phase is in 3 phase of movement. If the coefficient of the time control is great, a movement based on current is used as (72) [22, 23]:

$$x_i^{t+1} = x_i^t + r\left(x_{best}^t - \beta r' \mu^t\right), \quad (72)$$

When μ^t is is the population mean. If not, the candidate is passively or actively moved towards a random candidate. A trial point is glued to the variable bounds was strictly adhered to and only accepted when it decreased J. The calculation coefficient of time control in the implementation is as (73):

$$c_t = \left|\left(1 - \frac{t}{T_{max}}\right)(2r - 1)\right|. \quad (73)$$

The Gradient Based Optimizer phase will be started using the JS population and the top JS candidates will be immediately assigned to the first elite positions. The remaining candidates are left so as to maintain diversity of the population. The updated GBO (adaptive coefficient) is implemented.

$$\beta_t = 0.2 + (1.2 - 0.2)\left[1 - \left(\frac{t}{T_{GBO}}\right)^3\right]^2, \quad (74)$$

and an oscillation coefficient as (75):

$$\alpha_t = \left|\beta_t \sin\left(\frac{3\pi}{2} + \sin\left(\frac{3\pi\beta_t}{2}\right)\right)\right|. \quad (75)$$

A gradient search perturbation is created from the best and worst individuals in the population and a difference mutation component is created from a subset of individuals chosen at random from the population for each candidate. The resulting trial candidate is then clipped to the bounds and it is only accepted if its penalized objective is better. The present implementation is also based on the adaptive population perturbation which was performed in the MATLAB GBO routine; thus, The applied GBO variant was called "applied GBO" instead of being an exact copy of all published GBO formulations. The hybrid algorithm uses a total number of iterations that are split into two consecutive phases as (76):

$$T_{JS} = \text{round}\left(\omega_{JS} T_{max}\right),\ T_{GBO} = T_{max} - T_{JS}, \quad (76)$$

with $\omega_{JS} = 0.60$. The elite fraction is $\omega_G = 0.50$, thus the top 50% of the JS population gets to propagate the GBO population. All 5 algorithms have the same population size, number of iterations and budget for objective evaluation. The number of iterations used for the reported comparison is 3630, the number of object evaluations per independent run, and the total iteration budget is 120, with the population size being 30. The final design reported for JS-GBO is the best feasible solution obtained among the independent JS-GBO runs as (77):

$$x_{opt} = \text{argmin}_{x \in \mathcal{F}} J(x), \quad (77)$$

The feasible design set is denoted as where $\mathcal{F}$. The performance indicators are determined by analysing the final design in the same thermal, hydraulic, exergy and economic model.

Results of the optimization are compared to the results of the standalone JS, the standalone GBO, the real-coded genetic algorithm, and particle swarm optimization. The comparison is based on the "best value", "mean value", "standard deviation (20 independent runs)", "computational time", "convergence behaviour" and "equal objective-evaluation budget". The comparison is not supposed to conclude that one metaheuristic is superior to the rest, but rather it should be seen as an evaluation of the performance of the adopted metaheuristic and parameters. [17, 20, 22, 23].

3.8 Annual equivalent-operating-hours simulation

Data for the annual assessment is provided by the daily NASA POWER data of irradiation and ambient temperature for Baghdad in 2020. The daily irradiation is converted to an equivalent daytime irradiance for each day, based on (78):

$$G_d = \frac{H_d \times 1000}{H_{sun}}, \quad (78)$$

The daily solar irradiation H_d received at any given day and location in kWh·m^{-2}·day^{-1} is calculated, where $H_{sun} = 5.5$ h·day^{-1} is the adopted equivalent sunshine duration. The daily operating time at the aggregation is then as (79):

$$\Delta t_d = \frac{H_d \times 1000}{G_d}. \quad (79)$$

The annual amounts are calculated by taking the steady-state model for each of the daily weather records and adding them up. This procedure is performed as an annual equivalent operating hours simulation that is based on daily data and not on a 24-hour simulation transient. In the absence of the weather file, a synthetic weather fallback series is created. Results from this alternate series should not be used to report as NASA POWER-based results [23].

3.9 Numerical verification

The last candidate only gets accepted if the feasibility flag is true. Also, the residual, in the form of a number, is presented for the final design as the energy-balance. There are two main requirements for verification as (80), (81):

$$|RE| \ll 1, \quad (80)$$

And

$$\Delta P \leq 47{,}500\ Pa, \quad (81)$$

$$T_{PV} \leq 85\ °C,\ \Delta T_{TEG} \geq 5\ K,$$

$$Re_{nf} \leq 10{,}000,\ P_{net} > 0,\ NPV > 0. \quad (82)$$

4. Results and Discussion

4.1 Optimal Solution

The model results are validated using the 366 daily weather dataset of the city of Baghdad for the year 2020 (PV/T–TEG model). A mean daily irradiation of 5.452 kWh·m^{-2}·day^{-1}, an annual irradiation of 1995.3 kWh·m^{-2}·year^{-1}, a design-point irradiance of 991.19 W·m^{-2}, and a mean ambient temperature of 24.60 °C are obtained. The economic and annual performance calculations are conducted using an equivalent annual operating period of 2013 h.

The optimal JS–GBO design is obtained at a nanofluid mass-flow rate of 0.04611 kg·s^{-1}, a collector area of 9.7906 m^2, a TEG hot-side temperature of 32.783 °C, and an Al_2O_3 concentration of 0.3397 vol.%. The resulting pressure drop is 47101.69 Pa, which is lower than the design limit of 47500 Pa and the physical limit of 50000 Pa. The optimum design yields an exergy efficiency of 17.5507%, a net electrical power output of 1468.47 W, and a useful thermal power output of 3374.44 W. The economic indicators are evaluated as an NPV of 1180.78 USD, an LCOE of 0.07932 USD·kWh^{-1}, and a simple payback period of 7.64 years. The relative energy-balance residual is constrained to 7.611 × 10^{-5}, which verifies the numerical consistency of the reported operating point. The optimized design decision variables, feasibility indicators and the main performance metrics are summarized in Table 3.

Table 3: Summary of the Optimal Operating Point Obtained by the JS–GBO Algorithm

Quantity	Value
Nanofluid mass-flow rate, $\dot{m}_{nf}$	0.04611 kg s^{-1}
Collector area, A_c	9.7906 m^2
TEG hot-side temperature, $T_{h,TEG}$	32.783 °C
Nanoparticle concentration, ϕ	0.3397 vol.%
Pressure drop, ΔP	47101.69 Pa
Design pressure-drop limit	47500 Pa
Physical pressure-drop limit	50000 Pa
Exergy efficiency, η_{ex}	17.5507%
Net electrical power, P_{net}	1468.47 W
Useful thermal output, $\dot{Q}_u$	3374.44 W
Net present value, NPV	1180.78 USD
Net levelized electricity cost, LCOE	0.07932 USD kWh^{-1}
Simple payback period, PBP	7.64 years
Relative energy-balance residual	7.611 × 10^{-5}

The climatic basis for the annual simulation is set in Fig. 3. An annual irradiation of 1995.3 kWh·m^{-2}·year^{-1} is obtained from the 366 daily records, and a mean daily irradiation of 5.452 kWh·m^{-2}·day^{-1} is calculated. These data are converted into a design irradiance of 991.19 W·m^{-2} and an equivalent operating time of 2013 h·year^{-1}.

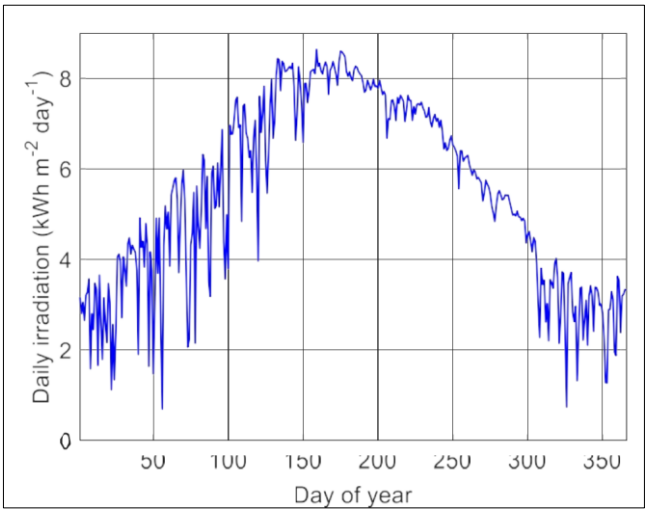


Fig 3: Baghdad Daily Irradiation Based on NASA POWER Data for 2020.

4.2 Comparison with Other Algorithms

The corrected implementation is compared with stand alone Jellyfish Search (JS), Gradient Based Optimizer (GBO), Genetic Algorithm (GA), Particle Swarm Optimization (PSO) and the proposed JS–GBO. All algorithms use the same number of individuals, iterations and number of evaluations of the objective function. There are 20 independent runs and in each run 3630 evaluations of the objective. Table 4 shows the statistical comparison of the optimization algorithms. The problem is set up as a minimization, so lower objective values mean better performance.

Table 4: Statistical Performance Comparison of the Optimization Algorithms

Algorithm	Best objective	Mean objective	Standard deviation	Mean evaluations	Mean time (s)
JS	−1.094257	−1.056510	0.03077	3630	2.067
GBO	−1.100026	−1.071804	0.02144	3630	3.956
GA	−1.105006	−1.072461	0.04564	3630	1.792
PSO	−1.105350	−1.104706	0.000736	3630	2.072
JS–GBO	−1.098234	−1.061193	0.02311	3630	2.549

The lowest mean objective value is obtained by PSO, with a value of −1.104706. The lowest variation is also achieved by PSO, yielding a standard deviation of 7.360 × 10^{-4}. The mean objective value obtained by the JS–GBO method on the feasible solution is higher than the mean objective values obtained by the GBO, GA, and PSO methods, namely −1.061193. Hence, JS–GBO is not claimed to be superior to all benchmark algorithms and is viewed as an effective and competitive hybrid technique under the considered scenarios. The mean curves of convergence for 20 independent runs are shown in Fig.4. The curves are compared with a fixed budget for evaluation of 3630 function evaluations per run. The result of the convergence behavior indicates that PSO has the lowest mean final objective while JS–GBO has a feasible but not dominant convergence result.

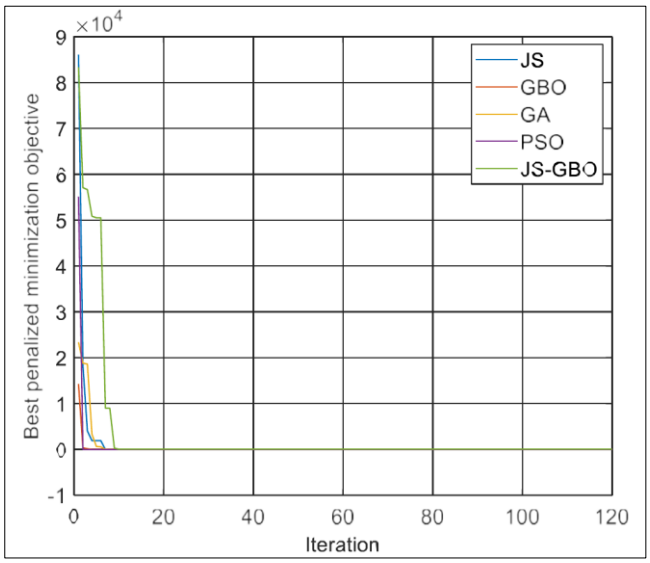


Fig 4: Mean Convergence of the Optimization Algorithms over Independent Runs.

Finally, the objective values and their spread are depicted in Fig. 5. The standard deviation of PSO is limited to 7.360 × 10^{-4}, whereas that of JS–GBO is 2.311 × 10^{-2}. Therefore, more stable results are achieved by PSO from run to run for the considered objective landscape.

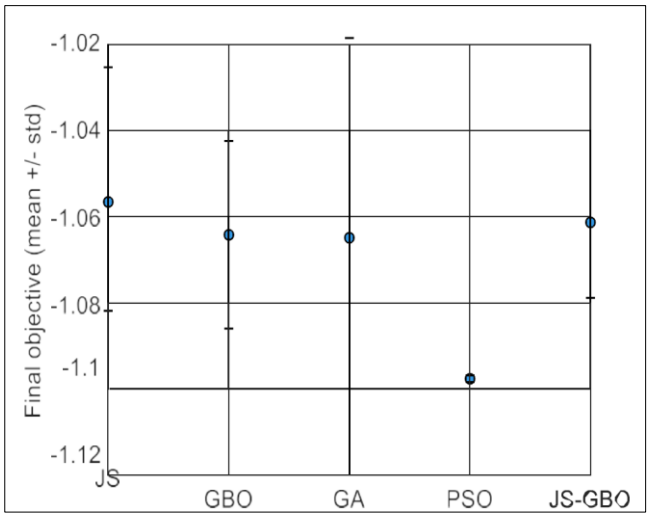


Fig 5: Robustness Comparison of the Optimization Algorithms.

Fig. 6 compares the normalized decision variables obtained by the five algorithms. JS–GBO solution features an intermediate flow rate, a large collector area, a low nanoparticle concentration, and a TEG hot side temperature of ~33 °C. The large selected collector area suggests a favourable target for expansion of the collection area within the set maximum limit.

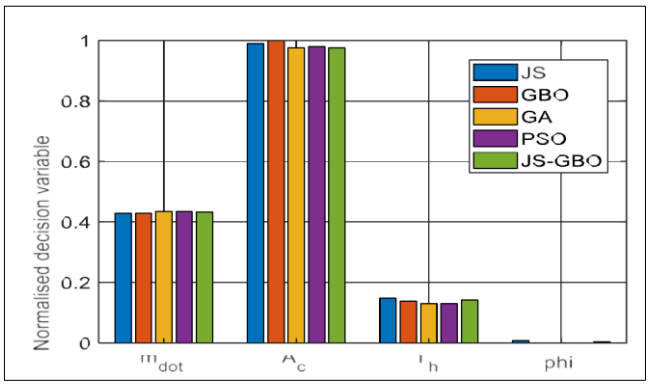


Fig 6: Decision Variables Obtained by the Optimization Algorithms.

4.3 Sensitivity Analysis

The sensitivity analysis is done by independently varying each decision variable around the feasible JS–GBO optimum. All other parameters are kept at their optimal values, and the mass-flow rate, collector area, TEG hot-side temperature and nanoparticle concentration are changed. This process is adopted to determine the significance of the variables in terms of the exergo-economic objective.

The effect of the nanofluid mass-flow rate is investigated in Fig. 7. Simultaneously, the flow rate influences the PV temperature, useful thermal energy output, exergy efficiency, pressure drop, and pumping power. The optimal value of 0.04611 kg·s^{-1} is adopted as a compromise between enhanced cooling and the hydraulic penalty resulting from the increased flow.

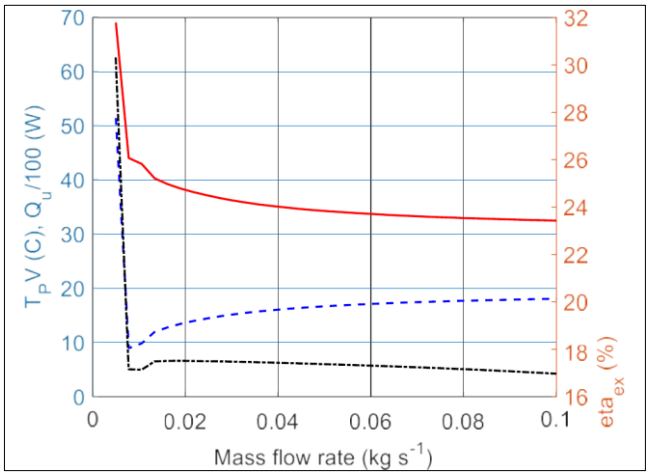


Fig 7: Flow-Rate Sensitivity of the PV/T–TEG System.

The effect of the concentration of nanoparticles is assessed using Fig.8. The chosen concentration of 0.3397 vol. % is near to the lower limit of 0.33 vol. %. This shows that the extra thermal gain that is gained with increased concentration of nanoparticles does not outweigh the combined viscosity, hydraulic, pumping and economic penalty for the model used.

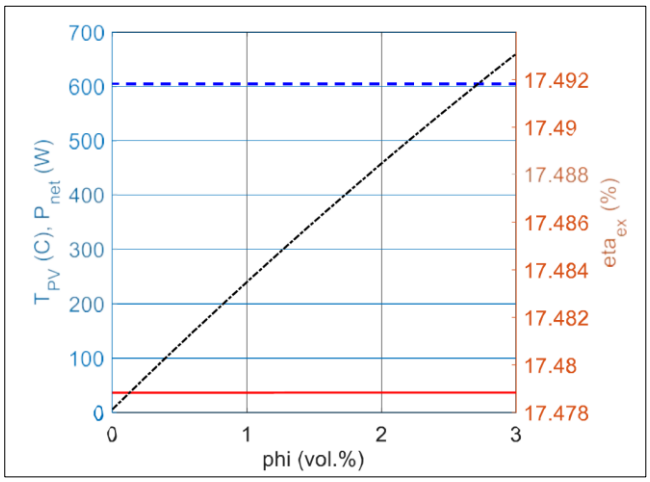


Fig 8: Nanoparticle-Concentration Sensitivity of the PV/T–TEG System.

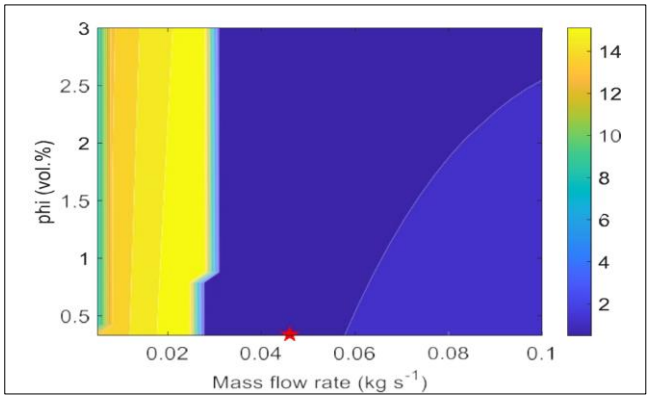


Fig 9: Feasible Exergo-Economic Objective Response Surface.

The sensitivity of the one-at-a-time design is shown in Fig. 10 around the optimized design. The sensitivity of the one-at-a-time design around the optimized design is shown in Fig. 10. In this context, the strongest response is expected from mass-flow rate and collector area as both have an impact on the heat transfer, electrical production, capital cost, and hydraulic losses. The local response is weaker for the nanoparticle concentration, as the optimum is close to the lower limit of the concentration range.

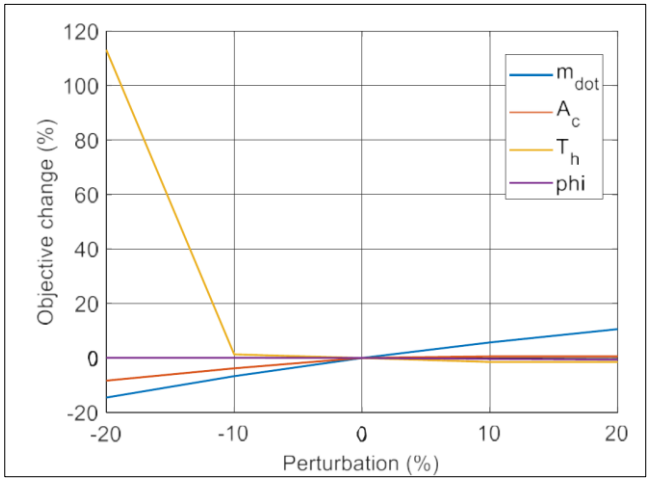


Fig 10: One-at-a-Time Sensitivity around the Optimum.

4.4 Energy Performance

The optimized design provides a net electrical power of 1468.47 W and a useful thermal output of 3374.44 W. The exergy efficiency is determined to be 17.5507%. The electrical power output after subtracting the pumping power from the combined PV and TEG power output is the net electrical power. Thus, electrical performance reported is subject to the hydraulic penalty and not just gross PV and TEG production.

The baseline electrical-power comparison is shown in Fig. 11. The PV output is referred to as the main electrical term, the TEG output is added as an additional recovery term and the pump output is considered as a parasitic consumption. The net electrical power is then calculated as the gross production minus the pumping requirement.

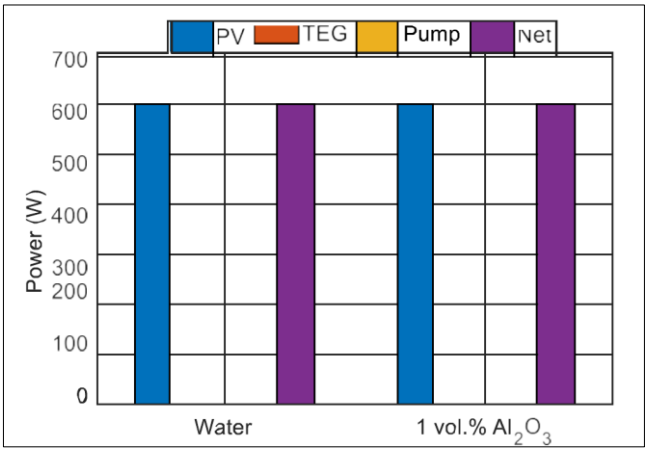


Fig 11: Baseline Electrical-Power Comparison between Water and Al_2O_3/Water Nanofluids.

The main energy and exergy quantities are summarized at the feasible optimum in Fig. 12. An exergy efficiency of 17.5507% is achieved, and the relative energy-balance residual of the thermal model is 7.611×10^{-5}. This residual value is less than 10^{-4}, which confirms the numerical consistency of the optimized energy flows.

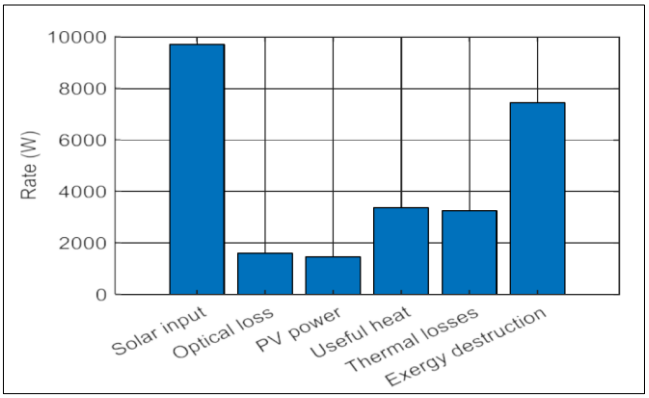


Fig 12: Optimal Energy and Exergy Quantities.

The annual performance is presented based on daily weather data in Fig. 13. The annual aggregation is done according to equivalent operating hours of daily irradiation and ambient temperature. Therefore, it is interpreted as a daily-data based annual simulation and not as a full transient 24-hour simulation.

4.5 Economic Performance

The investment cost, operation and maintenance cost, pumping-energy cost, electricity revenue, and useful-heat revenue are evaluated to study the economic performance, alongside the net present value (NPV), levelized cost of energy (LCOE), and simple payback period. A positive NPV of 1180.78 USD is achieved, and the simple payback period is calculated as 7.64 years. The net LCOE is determined as 0.07932 USD·kWh^{-1}, where the useful-heat revenue is subtracted from the annualized cost. The reported return indicator is defined in the numerical code as the NPV-to-investment ratio; it is thus designated as an NPV-based return indicator rather than an annual cash-flow return on investment (ROI) to avoid ambiguity between the two metric definitions.

The optimized design is depicted in Fig. 14 as a cumulative discounted cash flow. The NPV of the project over the evaluated lifespan is positive (NPV = 1180.78 USD), and the initial investment is recovered after 7.64 years based on the simple payback period calculation. The economic outcomes remain subject to the underlying assumptions regarding electricity price, thermal-energy credit, discount rate, component costs, and equivalent operating duration.

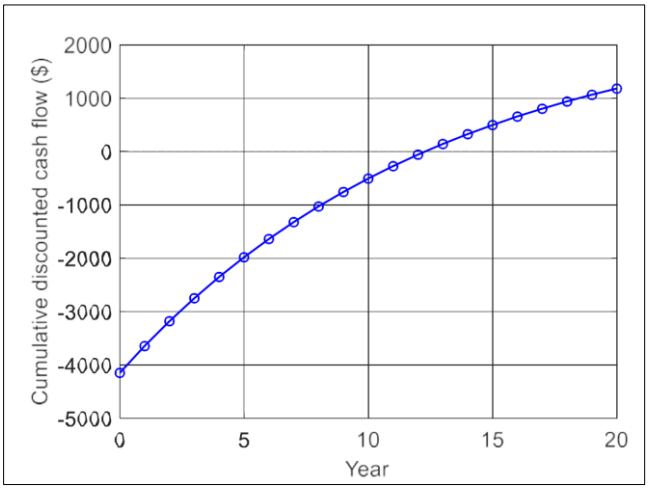


Fig 14: Discounted Cash Flow of the Feasible Optimum.

The exergy–economic trade-off gained from changing the objective weights is depicted in Fig. 15. Alternative feasible compromises among exergy efficiency, NPV, and LCOE are obtained by varying the weighting factors. The reported design does not represent the individual maximum of each performance indicator; rather, it reflects a compromise resulting from the reference weighting set ($w_1 = 0.4$, $w_2 = 0.4$, $w_3 = 0.2$).

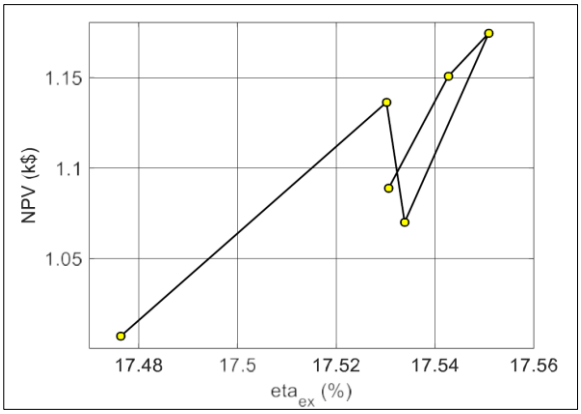


Fig 15: Exergy–Economic Trade-Off under Different Objective-Function Weights.

4.6 Nanofluid Impact

The effect of the Al_2O_3 concentration is evaluated through the temperature response, heat transfer response, hydraulic response, exergy response, and economic response. The concentration is adjusted within the range of 0.33 vol.% to 3.00 vol.%, which represents the optimization interval. The optimal value of 0.3397 vol.% is achieved near the lower boundary, indicating that operation with a low nanoparticle loading ratio is preferable when the overall exergo-economic objective is evaluated.

The calculated nanofluid properties and heat transfer responses are depicted in Fig. 16. Variations in thermal conductivity and viscosity as a function of concentration are assessed along with the convective heat transfer coefficient. The combined response demonstrates that high thermal conductivity alone is insufficient for achieving the optimum, as additional parameters—such as viscosity, Reynolds number, pressure drop, pumping power, and nanofluid cost—are simultaneously considered.

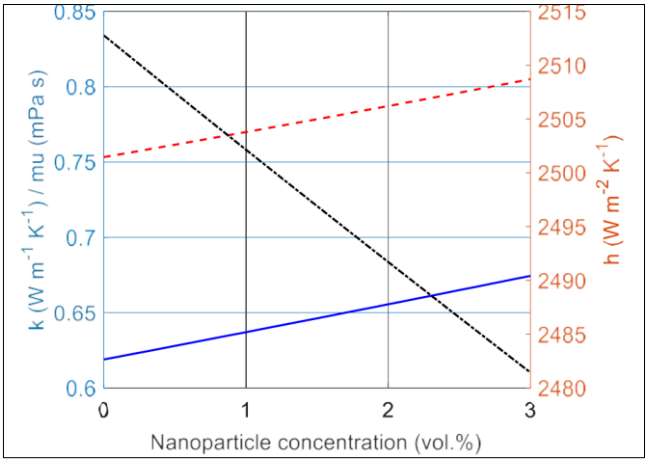


Fig 16: Nanofluid Properties and Heat-Transfer Coefficient as Functions of Nanoparticle Concentration.

The concentration effect on system performance is also shown in Fig. 8. The low optimized concentration signals that the added value of the nanoparticles in terms of thermal enhancement isn't economically and hydraulically beneficial with the assumptions used. Therefore, Nanofluid is used as the heat transfer enhancement medium not at the highest allowed concentration.

4.7 Convergence Behavior

The convergence behaviour is calculated with the best objective value found at every iteration. The comparison is based on 20 independent runs and the same 3630 objective-function evaluations are used for each algorithm. This design of equal budgets will avoid an apparent improvement due to an increase in the number of objective evaluations.

The mean convergence behaviour is plotted in Fig. 4. The PSO curve corresponds to the lowest mean final objective and the JS–GBO curve is feasible, yet not attaining the best average value. These results show that the new parameterization JS–GBO does not do better in the model adopted than PSO for the considered model.

The objective values are ultimately demonstrated to be robust, as depicted in Fig. 5. The smallest standard deviation of 7.360×10^{-4} is produced by PSO, whereas a standard deviation of 2.311×10^{-2} is yielded by JS–GBO. The lower variation exhibited by PSO indicates higher precision across different random initializations.

The algorithm comparison is thus considered as a model-specific benchmark. The results are neither a confirmation that PSO is always better nor a finding that JS–GBO is always worse; they simply indicate that the performance of the algorithms relative to each other is dependent on the objective landscape, the parameters used, the constraints and their treatment, and the evaluation budget.

4.8 Graphical Results and Tables

The graphical results are utilized to link the environment conditions, impacts on the decision variable, algorithmic behavior, energy performance, economic response and TEG operation. Climatic input is displayed in Fig. 3, while Fig. 7, Fig. 8, Fig. 9, Fig.11, & Fig. 16 quantify the nanofluid and operating-variable effects. Fig. 4, Fig. 5, Fig. 6 quantify the climatic inputs for the optimization methods, Fig. 12, Fig. 13quantify the energy and annual performance, Fig. 14, Fig. 15 quantify the economic and weighting-factor responses, and the TEG operating characteristic is displayed in Fig. 17. Fig. 17 presents the matched-load TEG power characteristic as a function of the TEG temperature difference. The temperature on the TEG hot-side that is optimized to evaluate the operating point is 32.783 °C. The TEG contribution is affected by the temperature difference available and by the thermal coupling between the absorber, TEG module and coolant. The TEG power is only counted in electrical out as the pumping power is subtracted.

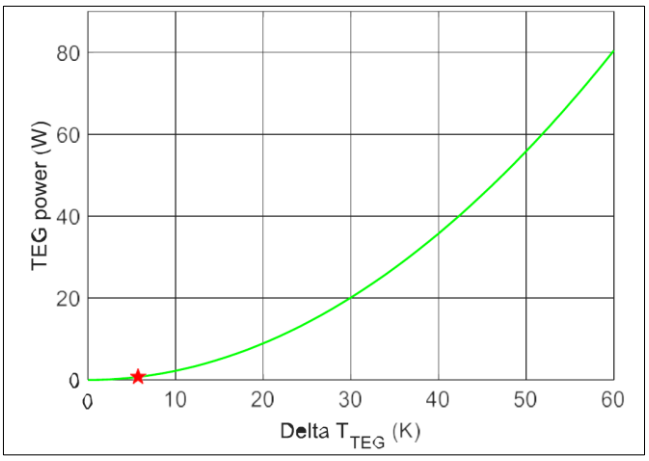


Fig 17: TEG Matched-Load Characteristic at the Optimum.

The optimized design and the algorithmic comparison are reported numerically in Table 3 and Table 4, respectively. These tables complement the graphical results by detailing the actual decision variables, feasibility limits, objective statistics, performance indicators, and computational budgets.

The modified formulation yields a JS–GBO model that is both numerically consistent and hydraulically feasible. An exergy efficiency of 17.5507%, a net electrical power of 1468.47 W, a useful thermal output of 3374.44 W, an NPV of 1180.78 USD, and a net LCOE of 0.07932 USD·kWh^{-1} are provided by the optimized solution. The pressure drop is maintained below the design limit, and the relative energy-balance residual is kept below 10^{-4}. However, the lowest mean objective value and the lowest run-to-run variation among the compared methods are achieved by PSO. Therefore, under the considered assumptions, JS–GBO is presented as a viable and competitive optimization technique, while no claim of universal superiority is asserted.

5. Conclusions & Recommendations

A constrained exergo-economic optimization model is developed for an Al_2O_3/water PV/T–TEG system, and a hybrid JS–GBO framework is implemented through coupled thermal, hydraulic, exergy, and economic calculations. A feasible design is obtained at a mass flow rate of 0.04611 kg·s^{-1}, a collector area of 9.7906 m^2, a nanoparticle concentration of 0.3397 vol.%, and a TEG hot-side temperature of 32.783 °C. An exergy efficiency of 17.5507%, an electricity output of 1468.47 W, and a useful thermal output of 3374.44 W are achieved. Furthermore, the pressure-drop constraint and the energy balance are satisfied, yielding an NPV of 1180.78 USD and an LCOE of 0.07932 USD·kWh^{-1}. The optimal mean objective value and the lowest variability for this dataset are achieved by PSO; thus, the universal superiority of JS–GBO is not demonstrated. Experimental validation, uncertainty analysis, expanded collector-area bounds, and multi-climate testing are recommended. Inclusion of transient hourly weather data, nanofluid stability and degradation effects, detailed TEG contact resistance, lifecycle environmental impacts, and multi-objective Pareto optimization is also required for future work.

References

1. Ibrahim A, Othman MY, Ruslan MH, Mat S, Sopian K. Recent advances in flat plate photovoltaic/thermal (PV/T) solar collectors. Renew Sustain Energy Rev. 2011;15(1):352-65. doi:10.1016/j.rser.2010.09.024
2. Manickam R, Babu MD, Babu MN, *et al*. Advancements in solar thermal collectors: integrating nanotechnology and design innovations for improved efficiency and sustainability. J Therm Anal Calorim. 2026;151:2033-62. doi:10.1007/s10973-025-15205-5
3. Madhi H, Aljabair S, Imran AA. A review of photovoltaic/thermal system cooled using mono and hybrid nanofluids. Int J Thermofluids. 2024;22:100679. doi:10.1016/j.ijft.2024.100679
4. Shahsavar A, Toghraie D. Experimental comparison of energy and exergy performances of photovoltaic/thermal systems containing mono, hybrid, and ternary nanofluids. Sol Energy Mater Sol Cells. 2026;296:114065. doi:10.1016/j.solmat.2025.114065
5. Celik Toker S, Kizilkan O. Thermodynamic, economic, and multi-objective optimization analysis of a solar tower-driven sCO2 Brayton-based multigeneration system. Energy Sources A Recovery Util Environ Eff. 2026;48(1). doi:10.1080/15567036.2026.2662542
6. Bjørk R, Nielsen KK. The performance of a combined solar photovoltaic (PV) and thermoelectric generator (TEG) system. Sol Energy. 2015;120:187-94. doi:10.1016/j.solener.2015.07.035
7. Nagasri DLS, Pathipooranam P, bin Mohd Salleh MF, Marimuthu R. Evaluating the performance and feasibility of integrating thermoelectric generators with solar photovoltaic panels: A case study. Case Stud Therm Eng. 2024;64:105572. doi:10.1016/j.csite.2024.105572
8. Yousif HS, Jalil SM. Evaluation of thermoelectric generators negative impact on hybrid PV-TEG system performance by using new proposed TEG model; computational and experimental analysis. Int Commun Heat Mass Transf. 2025;169:109843. doi:10.1016/j.icheatmasstransfer.2025.109843
9. Madhi H, Aljabair S, Imran AA. A review of photovoltaic/thermal system cooled using mono and hybrid nanofluids. Int J Thermofluids. 2024;22:100679. doi:10.1016/j.ijft.2024.100679
10. Aziz A, Sultan W, Shabbir H, *et al*. Advancements in photovoltaic thermal cooling systems: analysis of nanofluid technologies. J Therm Anal Calorim. 2026;151:6343-69. doi:10.1007/s10973-026-15430-6
11. Prasetyo SD, Trisnoaji Y, Arifin Z, Prabowo AR. Enhancing thermal efficiency of Photovoltaic/Thermal (PV/T) collectors: A systematic review and meta-analysis on fin geometry modifications and nanofluid applications. Unconv Resour. 2026;11:100352. doi:10.1016/j.uncres.2026.100352
12. Samarth AB, Nanvala H. Performance Evaluation of Polycrystalline and Monocrystalline PV Modules Using Hybrid Nanofluid-Based Active Cooling. Adv Eng Intell Syst. 2026;5(3):67-75. doi:10.22034/aeis.2026.576388.1516
13. Al-Hamed KH, Dincer I. Exergoeconomic analysis and optimization of a solar energy-based integrated system with oxy-combustion for combined power cycle and carbon capturing. Energy. 2022;250:123814. doi:10.1016/j.energy.2022.123814
14. Nadweh S, Mohammed N, Mekhilef S. Optimized Small-Scale CCUS Systems for Emerging Economies: A Metaheuristic-Based Modeling Approach with Economic and Environmental Assessment. In: 2026 6th International Conference on Emerging Smart Technologies and Applications (eSmarTA); 2026; Dhamar, Yemen. p. 1-8. doi:10.1109/eSmarTA70636.2026.11652106
15. Mao Z, Zhou S, Khan MS, Jin W, Gao Z. Exergo-economic analysis and multi-objective optimization of a novel solar-driven multigeneration system for efficient energy utilization. Appl Therm Eng. 2025:127512. doi:10.1016/j.applthermaleng.2025.127512
16. Vafaeenezhad M, Abedini Esfahlani A, Rahbar N, Rafiei M, Jamshidi E. Recent Advances in Renewable Energy-Integrated Thermodynamic Cycles: A Comprehensive Review. J Heat Mass Transf Res. 2026;13(3):315-34. doi:10.22075/jhmtr.2025.37312.1718
17. Minai AF, Malik H. Metaheuristics Paradigms for Renewable Energy Systems: Advances in Optimization Algorithms. In: Malik H, Iqbal A, Joshi P, Agrawal S, Bakhsh FI, editors. Metaheuristic and Evolutionary Computation: Algorithms and Applications. Studies in Computational Intelligence, vol 916. Singapore: Springer; 2021. doi:10.1007/978-981-15-7571-6_2
18. Nadweh S, *et al*. Enhancing CDSS Performance with Advanced RNN Architectures and Data Augmentation Techniques. In: 2026 International Conference on Digital Transformation, Innovation & Sustainable Development (DTISD); 2026; Aden, Yemen. p. 1-8. doi:10.1109/DTISD69661.2026.11668106
19. Shibghatullah ASB, Bunyan ST, Nadweh S. Blockchain-Enabled Demand Response: Designing Consumer-Centric Electricity. In: Energy Informatics: 5th Energy Informatics Academy Conference, EIA 2025; Kuala Lumpur, Malaysia. Springer Nature; 2026. p. 177.
20. Nassef AM, Abdelkareem MA, Maghrabie HM, Baroutaji A. Review of metaheuristic optimization algorithms for power systems problems. Sustainability. 2023;15(12):9434. doi:10.3390/su15129434
21. Nadweh S, Mohammed N, Mekhilef S. Intelligent prediction of photovoltaic inverter failures for improved reliability and control in smart grid systems. Electr Power Syst Res. 2026;255:112735. doi:10.1016/j.epsr.2026.112735
22. Chou JS, Truong DN. A novel metaheuristic optimizer inspired by behavior of jellyfish in ocean. Appl Math Comput. 2021;389:125535. doi:10.1016/j.amc.2020.125535
23. Ahmadianfar I, Bozorg-Haddad O, Chu X. Gradient-based optimizer: A new metaheuristic optimization algorithm. Inf Sci. 2020;540:131-59. doi:10.1016/j.ins.2020.06.037

How to Cite This Article

Kadhim AN. Hybrid jellyfish search and gradient boosting optimizer for exergo-economic optimization of nanofluid-based PV/T systems integrated with thermoelectric generators. International Journal of Multidisciplinary Research and Growth Evaluation. 2026;7(4):867-882. doi:10.54660/IJMRGE.2026.7.6.231-246.

Creative Commons (CC) License

This is an open access journal, and articles are distributed under the terms of the Creative Commons Attribution NonCommercial-ShareAlike 4.0 International (CC BY-NCSA 4.0) License, which allows others to remix, tweak, and build upon the work non-commercially, as long as appropriate credit is given and the new creations are licensed under the identical terms